VLF Electric and Magnetic Fields Observed in the Auroral Zone with the Javelin 8.46 Sounding Rocket

DONALD A. GURNETT AND STEPHEN R. MOSIER[1]

Department of Physics and Astronomy
The University of Iowa, Iowa City, Iowa 52240

Results of the Javelin 8.46 VLF electric and magnetic fields experiment flown from Fort Churchill, Canada, on May 25, 1968, are discussed. This experiment carried three orthogonal magnetic loop antennas, three orthogonal long (3.16 meters) electric dipoles, two short (42 cm) electric dipoles, and six wideband (30 Hz to 10 kHz) receivers for amplifying signals from the various VLF antennas. Intense noise bursts with frequencies less than about 1.5 kHz were observed on all the electric antennas below 500-km altitude, but not on the loop antennas. The precession and spin modulation of these noise bursts suggest that the noise is generated by an interaction between the payload and the surrounding plasma. High-frequency electrostatic noise bursts, from 5 to 30 kHz, were observed throughout the flight. These noise bursts, similar in some respects to lower-hybrid-resonance noise commonly observed with satellite VLF electric field experiments, also appear to involve an interaction between the payload and the surrounding plasma. Attenuation bands at harmonics of the proton gyrofrequency were also found in the frequency spectra of electric field noise observed during a portion of the flight.

1. INTRODUCTION

This paper describes a very-low-frequency (VLF) electric and magnetic fields experiment flown on the Javelin 8.46 sounding rocket from Fort Churchill, Canada, and summarizes the amplitudes and frequency spectra of electrostatic and electromagnetic noise observed during the flight.

The scientific objectives of this experiment were to determine the amplitude and frequency spectra of naturally occurring electric and magnetic fields in the auroral zone over the frequency range from about 30 Hz to 10 kHz, to compare observed plasma wave phenomena with low-energy (5 ev to 50,000 ev) charged particle flux measurements on the same payload, and to investigate the performance of the electric dipole antennas by comparing the signals received with different types of electric dipole antennas.

The payload instrumentation used on this flight is very similar to the VLF electric and magnetic field experiment flown on the Javelin 8.45 sounding rocket from Wallops Island, Virginia, in September 1967, and described by *Shawhan and Gurnett* [1968].

2. DESCRIPTION OF INSTRUMENTATION

The payload instrumentation consists of eight antennas and six receivers for the detection of VLF electric and magnetic fields and an electrostatic analyzer for the measurement of electron and proton fluxes in the energy range from 5 ev to 50,000 ev. The electrostatic analyzer is a low-energy proton and electron differential energy analyzer (LEPEDEA) of the type described by *Frank* [1967]. Figure 1 illustrates the mechanical arrangement of the various VLF antennas on the payload. Two different length electric dipole antennas are used. The long electric dipoles, parallel to the x and y axes, are of the type described by *Storey* [1965], each consisting of two spherical antenna elements 15.3 cm in diameter with a center-to-center separation of 3.16 meters. Two different types of spheres are used, solid conducting spheres for the y-axis elements, and approximately 90% transparent wire gird spheres for the x axis elements. The z-axis antenna consists of a conducting conical element, 18 cm in diameter and 13 cm high, on the end of the z-axis boom (see Figure 1). The second element of the z-axis antenna consists of the conducting rocket body. The center-to-center separation between the conical z-axis element and the rocket body

[1] NASA Graduate Trainee.

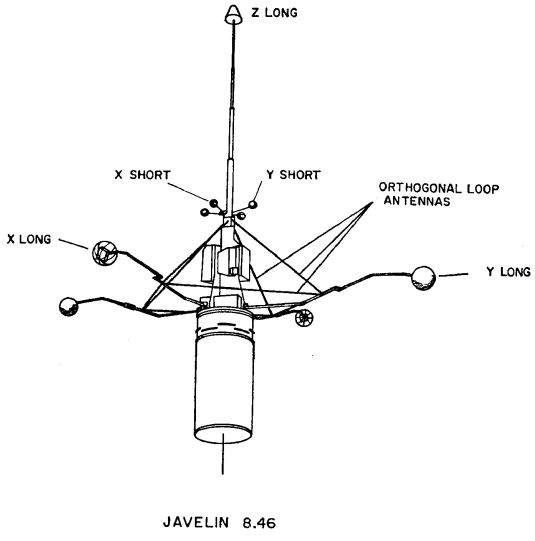

Fig. 1. Sketch showing the relative orientation and location of the VLF antennas.

is approximately 3 meters. The booms supporting these antenna elements are insulated from the payload and the spheres and are coated with a nonconducting paint to insulate the booms from the surrounding plasma. The short electric dipoles, parallel to the x and y axes, are similar to the long antennas except for the dimension. The center-to-center separation between the short dipole antenna spheres is about 42 cm, and the diameter of the spheres is 7.6 cm. Since the potential difference between the spheres, for long wavelength electric fields, is proportional to the antenna length, measurements from a parallel set of long and short antennas can be used to confirm that observed potential fluctuations are due to long wavelength electric fields. The solid and grid spheres are used to compare resistive versus capacitive coupling of the spheres to the surrounding plasma.

A high input impedance unity gain preamplifier is located inside each of the large spheres to provide signals to the main payload electronics proportional to the sphere potential. The input impedance of the preamplifiers is very large and can be represented by a 20-megohm resistance in parallel with a 10-pf capacitance. The booms are driven by the output from the unity gain preamplifier to reduce the capacitance between the sphere and the boom. The noise level of these preamplifiers is about 10^{-13} volt^2/Hz. The unity gain preamplifiers for the small spheres are located at the base of the small sphere booms and have an input impedance that can be represented by a 100-megohm resistor in parallel with a 3-pf capacitance. The noise level of these preamplifiers is about 10^{-12} volt^2/Hz.

The three orthogonal magnetic loop antennas used for detecting magnetic fields are shown in Figure 1. Each loop consists of two turns of #14 stranded copper wire and is electrostatically shielded. The z-axis loop is a square loop with an area of 1.6 meters^2 running between points approximately half-way out the x- and y-axes booms. The x- and y-axes loops are triangular loops, with areas of 0.8 meters^2, running from the top of the payload to the booms and back through the payload. The loops are matched to the preamplifiers by a transformer with a 200:1 turns ratios. The sensitivity of the magnetic antenna system is approximately $2.5 \times 10^{-4}/f^2$ (gamma^2/Hz), where f is the frequency in hertz.

Signals from the antennas are processed in two frequency bands, 30 to 650 Hz, hereafter referred to as the 'low' band, and 650 Hz to 10 kHz, hereafter referred to as the 'high' band. The ac signal in each band is logarithmically compressed and transmitted to the ground broadband so that high resolution frequency-time spectra can be obtained. Also a dc voltage proportional to the logarithm of the signal strength in each band is telemetered to the ground so that the field intensities in each high and low band can be determined. These field intensity measurements cover an 80-db dynamic range and are made at a rate of approximately 3 samples/second for each band. Because of the large number of antennas used, it is necessary to commutate some of the electric antennas with the available receivers. The commutation sequence used consists of switching the E_x-short antenna in place of the E_x-long antenna, and the E_y-short antenna in place of the E_z-long antenna for 8 seconds out of every 32 seconds. In addition to the high- and low-band field strength measurements, narrow-band field strength measurements are also performed for the E_x-long antenna at 7.35, 10.5, 14.5, 22.0, 30.0, 40.0, 52.5, and 70.0 kHz with bandwidths of $\pm 7.5\%$.

3. Trajectory, Launch Conditions, and Payload Operation

A. *Trajectory*

The Javelin 8.46 payload was launched at 05h 18m 48s UT, May 25, 1968, from Fort Churchill, Canada, (23h 18m 48s local time, 70.1° invariant latitude). The payload reached a peak altitude of 801 km and impacted approximately due east (azimuth, 87.9°) of Fort Churchill, 511 km from the launch site. The total flight time was 961 seconds.

B. *Launch Conditions*

The intended launch objective was to fire the rocket so as to pass over a homogeneous auroral arc and to study a type of radio noise called VLF hiss that commonly occurs in association with homogeneous auroral arcs [*Morozumi,* 1963; *Gurnett,* 1966]. The rocket was successfully launched with an auroral arc under the flight trajectory as determined visually from the launch site. The aurora was observed to remain under the trajectory throughout the flight. Unfortunately, because of the twilight conditions that existed at night during late May at Fort Churchill, the all-sky camera records were of such poor quality as to prohibit a quantitative determination of the location of the aurora in relation to the flight trajectory. The LEPEDEA charged particle detector on board the payload did, however, detect intense fluxes ($\sim 10^8$ particles/cm^2 ster kev) of low-energy protons (100 ev — 10 kev) during the flight that are presumed to be responsible for the auroral light emission (L. A. Frank, personal communication) observed visually. No significant disturbances were observed on either the ground riometer or magnetometer records throughout the flight.

C. *Payload Operation*

At an altitude of approximately 230 km the four transverse, x and y axes, booms opened and locked in the extended position, as indicated by the appropriate microswitch closures telemetered to the ground. The z-axis antenna, which was erected approximately 10 seconds after the x and y-axes booms were opened, apparently did not lock in the fully extended position, as evidenced by the absence of the appropriate microswitch closure. The z-axis boom is, however, believed to have erected to nearly full length because of the large perturbation of the payload spin that occurred at the time when the z-axis boom was to be erected, and because the z-axis electric field intensities subsequently observed were very similar to the electric field intensities detected with the long x- and y-axes electric antennas.

Analysis of the triaxis magnetometer data indicated that the payload had a spin period of approximately 6.4 seconds about the z axis and that the spin axis was precessing around a cone of approximately 81.3° half-angle with a period of 11.84 seconds. The orientation of the precession cone was such that the z axis of the payload becomes nearly aligned and antialigned with the geomagnetic field once every precession cycle. The large precession apparently developed when the z-axis antenna was erected. Because of nulls in the transmitting antenna pattern in the positive z-axis direction, this unexpected end-over-end motion of the z-axis caused sharp fading to occur in the received telemetry data whenever the positive z axis is pointing downward toward the receiving station. Although these telemetry fades did not seriously impair the data analysis, they occurred throughout the flight and can be seen in most of the data presented in this paper.

At about 301 seconds after liftoff, at an altitude of 520 km on the upgoing part of the trajectory, one of the two transmitters on the payload failed abruptly for unknown reasons. The transmitter that failed was used to telemeter the field strength measurements and the LEPEDEA data. The remaining transmitter that telemetered the wide-band electric and magnetic field signals continued to operate properly throughout the flight.

4. Low-Frequency Electric Field Noise

Intense low-frequency electric field noise bursts, with frequencies below about 1.5 kHz, were detected on both the short and long electric antennas below about 500-km altitude. Figure 2 shows the low-band (30 Hz to 650 Hz) rms voltage difference between the spheres for the three orthogonal (E_x, E_y, and E_z) long electric antennas, and the two (E_x and E_y) short electric antennas during the upgoing portion of the flight. The switch indicator at the top of Figure 2 indicates whether the signal strengths

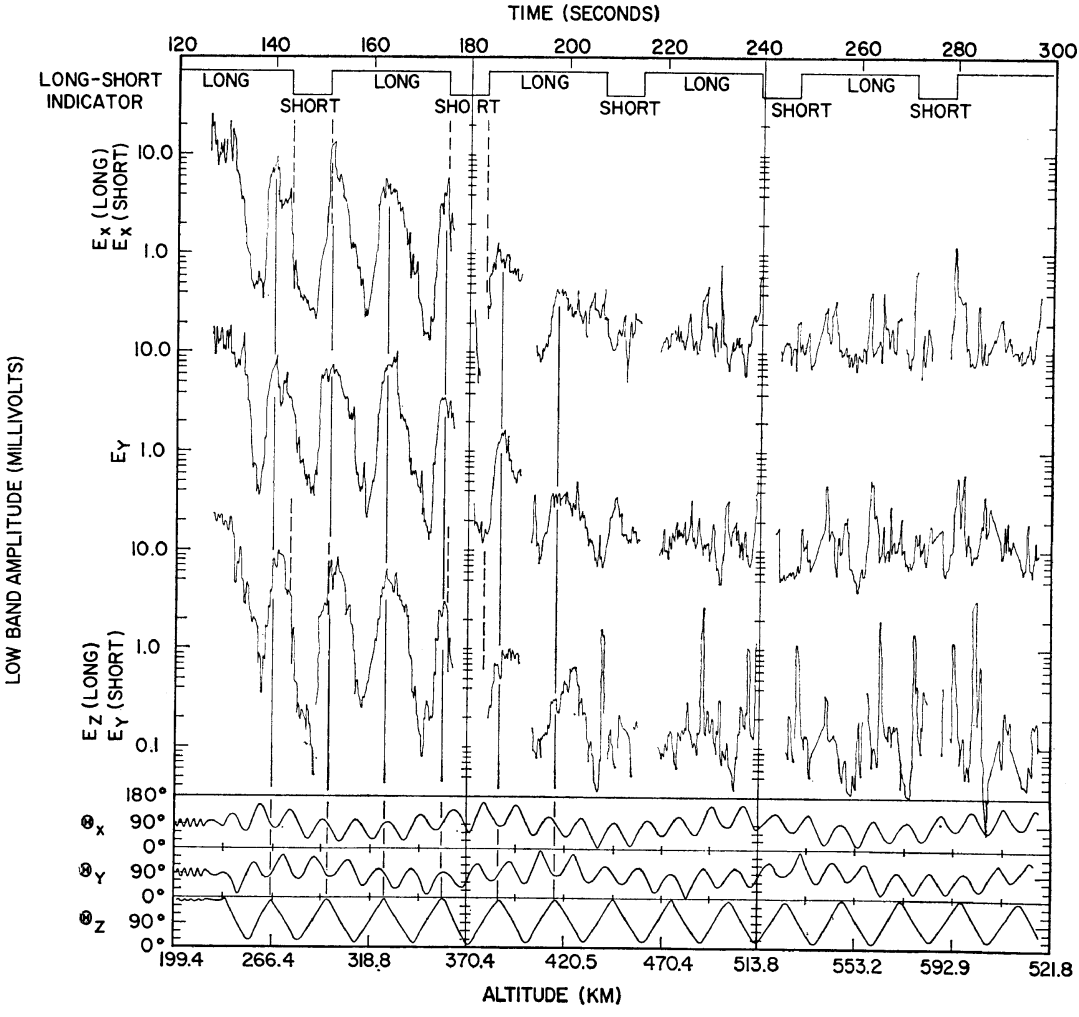

Fig. 2. Low-band electric field amplitudes.

are for the long or short antennas. Intense electric field noise bursts occurring periodically with peak intensities of the order of 30 mv are seen in Figure 2 on all the electric antennas from antenna deployment at 125 seconds up to about 210 seconds (all times refer to time from liftoff). The periodicity of these noise bursts correspond to the precession period of the z axis of the payload, as can be seen from the plot of the angle θ_z between the z axis and the geomagnetic field shown in the bottom of Figure 2. No comparable noise is observed with the magnetic loop antennas.

As can be seen from Figure 2 the electric field noise bursts occur essentially simultaneously on all antennas, and the peak noise intensity decreases systematically with increasing altitude. The rms noise voltage observed with the short E_y antenna can be compared with the corresponding noise voltage from the long E_y antenna from 143 to 151 seconds (see Figure 2). The noise voltage observed with the short antenna is typically about one-third of the noise voltage observed with the long antenna.

The frequency-time spectra of these precession-modulated noise bursts are shown in Figure 3 for all the electric antennas. The switching between the short and long antennas is indicated by the dark vertical line separating the x-short and x-long spectra, and the y-short and z-long spectra. This illustration shows that the precession modulation, θ_z dependence, is

essentially the same for all the antennas. The precession modulation pattern of this noise consists of a period during which the noise is undetectable, followed by a rapid onset with the upper frequency initially rising very rapidly. The 'envelope' of the noise burst is approximately symmetric about the time at which the z axis is parallel to the geomagnetic field.

To determine whether a parallel set of long and short antennas detected the same electric field signal, a correlation analysis was performed on signals from the E_y-short and E_y-long electric antennas from 175.5 to 180.0 seconds (see Figure 3) by filtering signals from each channel with identical filters (50-Hz bandwidth) and comparing the phases of the filtered signals at various center frequencies for the filter. Surprisingly, *no significant correlation was found* between the E_y-short and E_y-long antenna signals. Similar correlation measurements between pairs of long antennas and between the two short antennas yielded no correlation. Thus, even though the noise spectrum of the electric field observed by the different antennas is very

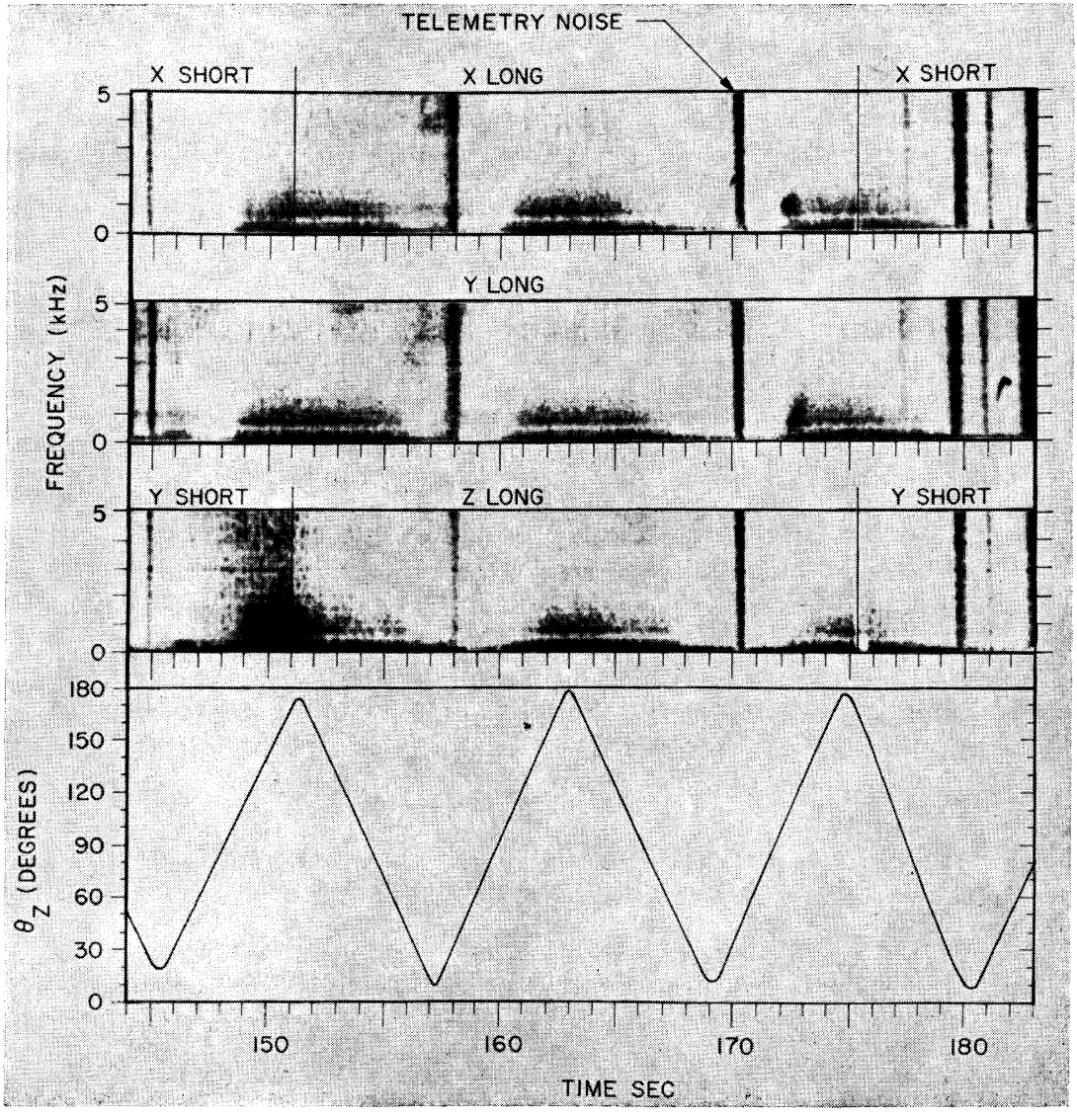

Fig. 3. Frequency spectra of the low-frequency electric field noise bursts.

similar, the correlation length of the electric field noise is apparently short compared with the antenna length.

Discussion

Low-frequency electric antenna noise very similar to the precession-modulated noise observed on this flight was also observed with the Javelin 8.45 VLF experiment launched at Wallops Island, Virginia [*Shawhan and Gurnett*, 1968]. Also, *Iwai et al.* [1966] have observed similar precession-modulated electric antenna noise in the frequency range from 0.5 to 3.5 kHz with the L-3-2 sounding rocket, and F. L. Scarf (personal communication) has observed possibly related noise phenomena with an electric field experiment on a Tomahawk rocket launched from Fort Churchill. These repeated observations indicate that this type of precession-modulated low-frequency electric antenna noise may be a characteristic feature of rocket-borne electric field measurements at low altitudes in the ionosphere. As of this time it is not known whether or not this type of electric field noise is also observed with satellite-borne electric field experiments.

1. *Origin.* In considering the origin of this precession-modulated noise, several factors strongly suggest that the noise is not a naturally occurring phenomena in the ionosphere, independent of the presence of the rocket. First, the orientation modulation of the noise intensity for the three orthogonal electric antennas, with an essentially identical 'on-off' intensity variation for *all three orthogonal antennas*, is inconsistent with any expected antenna pattern effect for the detection of ambient electrostatic waves. Antenna bias variations that possibly could simultaneously affect the coupling of all the antenna elements to the surrounding plasma can be shown to be negligible from measurements of the floating potential of the antenna elements obtained during the flight. Common-mode noise on the spacecraft body (coupled simultaneously to all the receivers through unbalanced antenna impedances) does not seem to be a possibility because of the poor correlation between signals from various antenna elements and the comparable noise intensity observed with the balanced x- and y-axes and unbalanced z-axis (which uses the payload body as one element of the antenna) antennas.

Second, the dependence of the noise intensity on the z-axis orientation of the payload suggests that the noise generation is somehow related to the physical asymmetry of the payload. Since the last stage rocket bottle, which is relatively large (approximately, 0.38 meters in diameter by 1.23 meters long), remained attached to the payload, the z-axis dependence suggests that the noise may be generated by an interaction between the rocket bottle and the surrounding plasma, possibly a wake effect or a plasma instability caused by currents produced from the $\mathbf{V} \times \mathbf{B}$ potential gradient of the conducting skin of the rocket bottle.

2. *Wavelength.* Several factors suggest that the wavelength of the low-frequency electric antenna noise is short compared with the length of the long electric antennas. First, the ratio of the noise voltages for the short and long E_y antennas is about 1 : 3. Since the length ratios of the short and long antennas is about 1 : 7.5, it is seen that the field intensity observed by the long antenna is too small by about a factor of 2.5 if the wavelength is long compared with the antenna length (electric field constant between the elements). This discrepancy can be accounted for if the wavelength is short compared with the long antenna length. Second, the relative phases of the electric field detected by the various dipole elements are uncorrelated. This lack of correlation can be accounted for only if the wavelength is short compared with the distance between the elements.

5. High-Frequency Electrostatic Noise

Electrostatic noise with frequencies from about 5 to 30 kHz was observed throughout the flight with all the electric dipole antennas. Typical frequency-time spectra of this noise are shown in Figures 4 and 5 at two different times during the flight.

During the early part of the flight from 480- to 579-km altitude, illustrated in Figure 4, this high-frequency electrostatic noise appears as a series of noise bursts, each burst lasting about 5 seconds and correlated with the z-axis orientation of the payload. The noise bursts occur essentially simultaneously on all the electric antennas as the angle between the z axis and the geomagnetic field decreases from about 180° to about 20° (see Figure 4). The noise intensity for all the long electric antennas is about 0.5

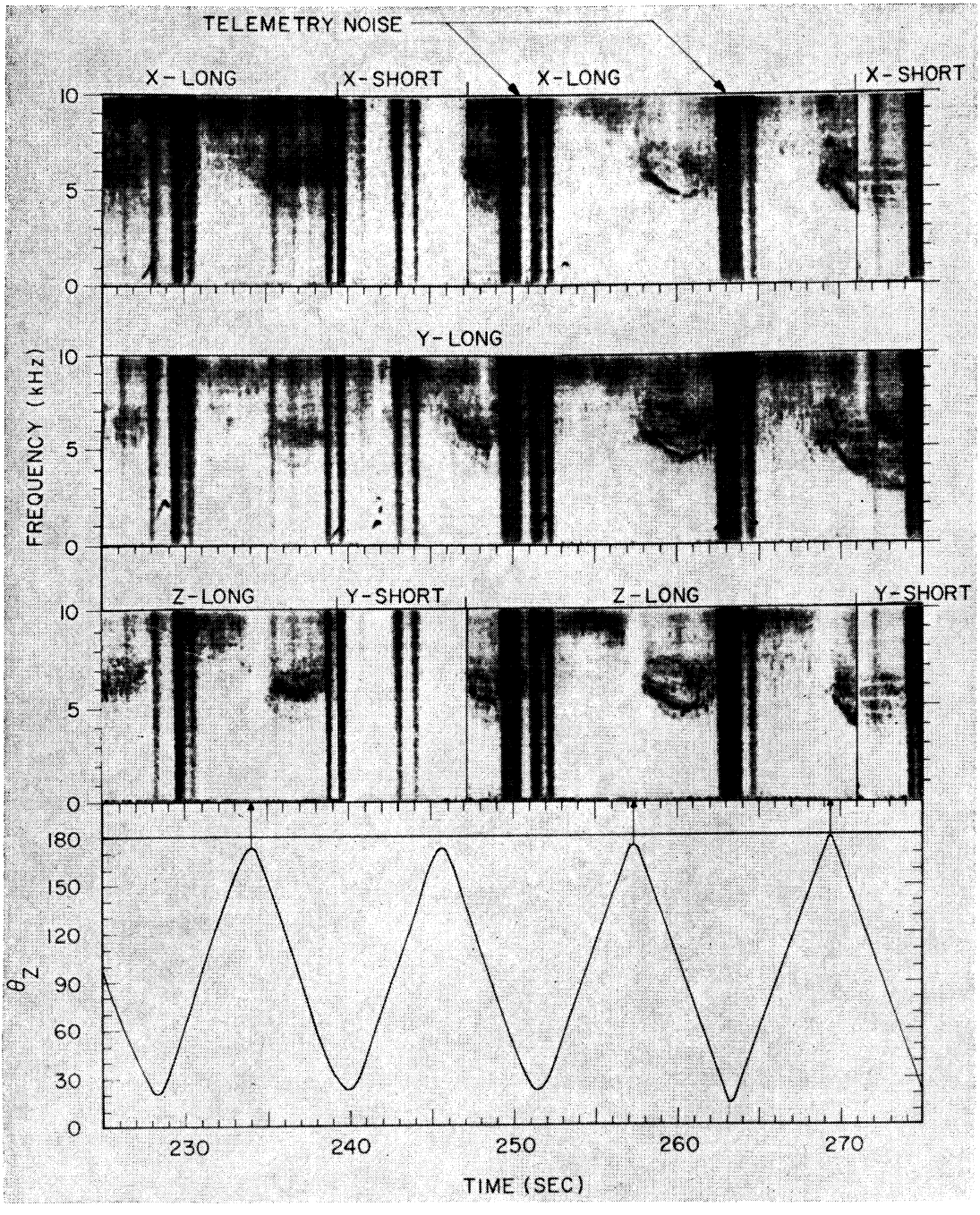

Fig. 4. Frequency spectra of the high-frequency electric field noise observed early in the flight.

to 1.0 mv ac potential difference between the elements. For the short electric antennas the noise is almost undetectable, probably because of the decreased sensitivity of the shorter antennas. Since no magnetic component could be detected with the loop antennas, we conclude that the noise is electrostatic (no magnetic field), to within the sensitivity limit of the mag-

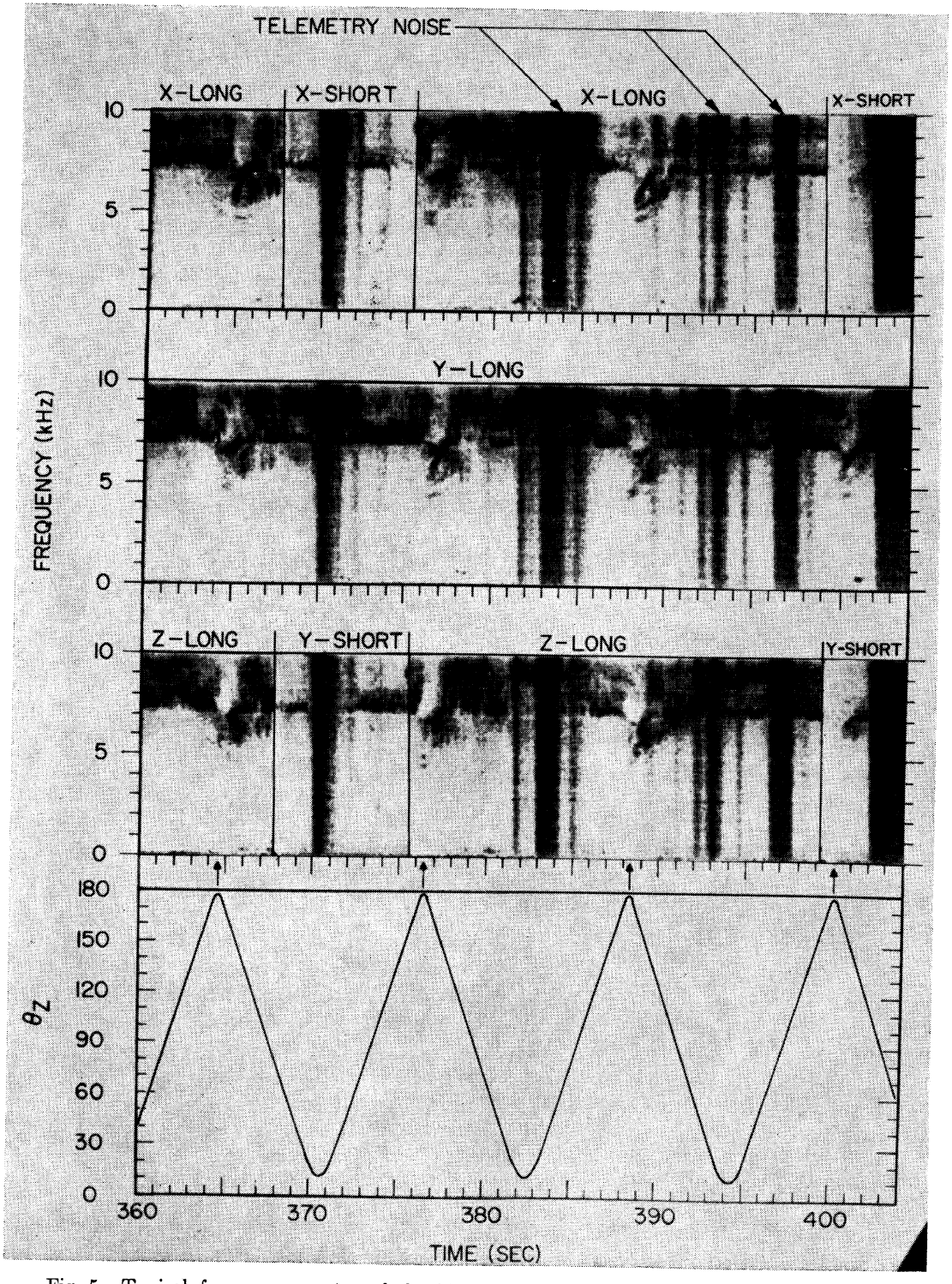

Fig. 5. Typical frequency spectra of the high-frequency electric field noise observed after about 280 seconds.

netic receivers used. The frequency-time spectra of the noise bursts shown in Figure 4 have considerable fine structure, sometimes consisting of closely spaced tones giving the noise bursts a characteristic 'finger print' appearance on the frequency-time spectrograms. From about 270 to 275 seconds in Figure 4 several distinct frequency bands appear in the frequency-time spectra that are associated with harmonics of the proton gyrofrequency (see discussion in the next section). From the step-frequency receiver data the noise spectral density is peaked at about 30 kHz below 420-km altitude, decreasing to about 22 kHz at 520-km altitude, at which point the transmitter failed and no further amplitude data could be obtained.

At an altitude of about 600 km (about 280 seconds) on the upgoing portion of the trajectory, the noise bursts shown in Figure 4 appear to gradually merge into a nearly steady band of noise with a sharply defined lower cutoff frequency similar to that shown in Figure 5 later in the flight. The frequency-time spectra of this high-frequency electrostatic noise band remain qualitatively similar to that shown in Figure 5 for the remainder of the flight. As illustrated in Figure 5 the noise spectrum continues to display a dependence on the z-axis orientation of the payload consisting of sharp nulls in the noise intensity of *all* the electric antennas when the z axis of the payload is pointing upward, parallel to the geomagnetic field ($\theta_z = 180°$, see Figure 5). The lower cutoff frequency of the noise band varies systematically during the downward portion of the flight, from about 6.8 kHz at apogee (801-km altitude) to about 8.0 kHz at about 300-km altitude where the noise gradually disappears. The broadband (650 Hz to 10 kHz) noise intensity during the downward portion of the flight, as estimated from the frequency-time spectrograms, is comparable with the intensity observed during the upgoing portion of the flight before the transmitter failure.

Discussion

In comparing these observations with results from other experiments, it is evident that certain features of the high-frequency electrostatic noise band observed on this flight are very similar to the lower-hybrid-resonance (LHR) noise observed at high latitudes with electric dipole antennas on the Alouette 1 and 2, and OGO 2 satellites [*Barrington et al.*, 1963; *Brice and Smith*, 1964, 1965; *McEwen and Barrington*, 1967; *Laaspere et al.*, 1969]. The specific points of comparison are as follows. First, LHR noise observed with satellites is generally electrostatic, since it is seldom observed with magnetic loop antennas [*Gurnett*, 1968; *Laaspere et al.*, 1969], as is the high-frequency electrostatic noise observed with this experiment. Second, LHR noise observed with satellites usually has a sharply defined lower cutoff frequency, believed to be the LHR frequency of the ambient plasma. The lower cutoff frequency of the high-frequency electrostatic noise observed during the latter portion of this flight (after 300 seconds) is in the approximate range (4 to 10 kHz) of the expected LHR frequency in the auroral zone for the altitude range of this flight. During the early portion of the flight, however, the frequency spectrum, orientation dependence, etc., of the high-frequency electrostatic noise are not comparable to any satellite observations of LHR noise.

1. *Origin.* Probably the most striking feature of the high-frequency electrostatic noise is the similar z-axis orientation dependence observed on all the electric antennas. Much as for the low-frequency electrostatic noise discussed in the previous section, this orientation dependence cannot be explained by any expected antenna pattern effect for the detection of ambient electrostatic waves. The dependence of the noise spectrum and intensity on the z-axis orientation of the payload suggests that the noise may be generated by an interaction between the payload and the surrounding plasma. Since this noise may be related to the LHR noise observed by satellites, this is the first evidence suggesting that the LHR noise observed by satellites may *not* be a natural noise phenomena in the ionosphere, but may, in fact, be generated by an interaction between the spacecraft and the surrounding medium.

6. Proton Gyrofrequency Harmonics

From approximately 270 to 282 seconds during the upgoing portion of the flight, a series of attenuation bands at harmonically related frequencies occurred in the noise bursts as shown in Figure 4. A preliminary report of these data has been published by *Mosier and*

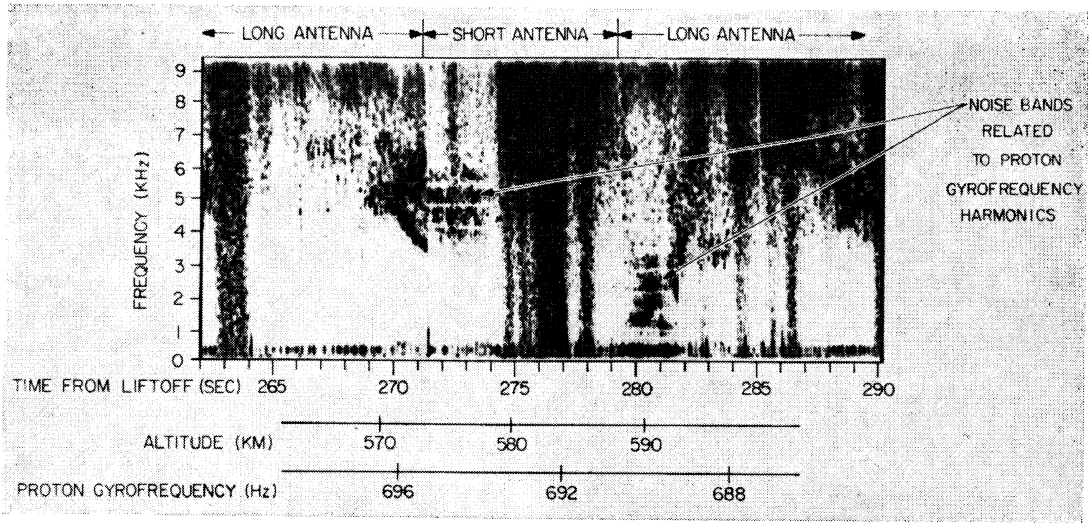

Fig. 6. Attenuation bands at harmonics of the proton gyrofrequency.

Gurnett [1969]; in this section, a more detailed discussion will be presented. The attenuation bands, shown with an expanded frequency-time scale in Figure 6, are each about 100 Hz wide and are located at frequencies corresponding to harmonics of the proton gyrofrequency, up to the eighth harmonic.

The upper and lower cutoff frequencies of each attenuation band were measured from further expanded frequency-time spectrograms and are given in Table 1. The error limits given reflect the estimated uncertainty in determining the cutoff frequencies from the spectrograms, the cutoff frequencies being defined as the frequency at which the noise intensity is reduced by about 10 db from the adjacent noise band. The proton gyrofrequency, f_{gp}, at the position of the payload was calculated from the *Jensen and Cain* [1962] spherical harmonic expansion for the geomagnetic field. The harmonics of the proton gyrofrequency are given in Table 1 for comparison with the corresponding cutoff frequencies. The error limits given for the proton gyrofrequency harmonics (±1%) are due to accuracy limitations of the Jensen and Cain expansion for the geomagnetic field and have been estimated from previous proton gyrofrequency measurements [*Gurnett and Shawhan*, 1966].

TABLE 1. Frequencies of Attenuation Bands and Corresponding Proton Gyrofrequency Harmonics

Cutoff Frequency, Hz		Harmonic of Proton Gyrofrequency, Hz
Lower	Upper	
	271 to 274 Seconds (f_{gp} = 694.3 Hz ± 1%)	
3448 ± 25	3619 ± 16	$5f_{gp}$ = 3471 ± 34
4173 ± 25	4258 ± 25	$6f_{gp}$ = 4165 ± 41
4883 ± 30	4987 ± 25	$7f_{gp}$ = 4860 ± 48
5356 ± 40	5650 ± 35	$8f_{gp}$ = 5554 ± 55
	280 to 281 Seconds (f_{gp} = 690.2 Hz ± 1%)	
*	827 ± 42	f_{gp} = 690 ± 7
1326 ± 20	1360 ± 13	$2f_{gp}$ = 1380 ± 14
2022 ± 25	2099 ± 35	$3f_{gp}$ = 2070 ± 21
2647 ± 37	3800 ± 37	$4f_{gp}$ = 2760 ± 28

* Could not be determined from data.

Comparing the observed cutoff frequencies with the harmonics of the proton gyrofrequency, as given in Table 1, it is seen that the proton gyrofrequency harmonics are generally within the attenuation bands. This conclusion is illustrated in Figure 7, which shows the relationship between the upper and lower cutoff frequencies of each attenuation band, the adjacent noise bands, and harmonics of the proton gyrofrequency.

Discussion

Effects at gyrofrequency harmonics are well known for a hot plasma with a static magnetic

field [*Gross*, 1951; *Bernstein*, 1958; *Stix*, 1962; and others]. The basic harmonic interaction mechanism can be illustrated by considering the electric field force, F, of a wave

$$F \propto \exp [ikx - i\omega t]$$

which is acting on a thermal particle orbiting in a static magnetic field. (Let the x axis be perpendicular to the static magnetic field.) Since the zero-order x-axis motion of the particle is $x = R_\perp \sin \omega_g t$ ($R_\perp$ = gyroradius, ω_g = gyrofrequency), we have

$$F \propto \exp [ikR_\perp \sin \omega_g t - i\omega t]$$

which by a well-known Bessel function identify [*Watson*, 1922] can be written

$$F \propto \sum_{n=-\infty}^{\infty} J_n(kR_\perp) e^{i(n\omega_g - \omega)t}$$

where J_n is the nth-order Bessel function. It is seen from the above expression that resonance effects occur at all the gyrofrequency harmonics ($n\omega_g - \omega = 0$). The 'strength' of the harmonic interaction, $J_n(kR_\perp)$, is controlled by the ratio of the gyroradius to the wavelength perpendicular to the static magnetic field, $\sim kR_\perp$.

For electrostatic waves propagating perpendicular to the static magnetic field, *Bernstein* [1958], considering the collective effects of all the particles for a Maxwellian velocity distribution, has shown that the dispersion relation consists of an infinite number of branches, with each branch bounded by adjacent gyrofrequency harmonics. These 'Bernstein modes' have been extensively investigated by a number of authors [*Stix*, 1962; *Crawford*, 1965; *Fredricks*, 1968]. For non-Maxwellian velocity distributions, such as a beam of particles gyrating about the static magnetic field, the Bernstein modes readily become unstable [*Crawford*, 1965] leading to noise emission in bands associated with the gyrofrequency harmonics.

Radiation from laboratory plasmas at harmonics of the electron and ion gyrofrequency has been reported and studied by several investigators, including *Landauer* [1962], *Bekefi et al.* [1962], *Tanaka and Kubo* [1964], and *Yamamota and Suita* [1968]. *Crawford and Weiss* [1966] have experimentally investigated the propagation of electrostatic electron cyclotron harmonic waves across a magnetic field in a laboratory plasma and have provided an excellent verification of the dispersion relation derived by Bernstein. Similar propagation effects at harmonics of the electron gyrofrequency have been observed in the ionosphere with the ionospheric sounder on the Alouette satellites [*Calvert and Goe*, 1963; *Fejer and Calvert*, 1964; *Sturrock*, 1965]. *Sato et al.* [1967] have investigated the propagation of electrostatic ion cyclotron wave in a laboratory plasma.

With this background of known plasma wave phenomena associated with gyrofrequency harmonics, it is not surprising that noise associated with harmonics of the proton gyrofrequency is observed in the ionosphere. The effects observed at harmonics of the proton gyrofrequency during this flight are to our knowledge the first confirmed observations of ion gyrofrequency harmonic effects in the ionosphere.

1. *Cutoff frequencies.* For a Maxwellian velocity distribution, *Fredericks* [1968] has shown that if a stop band occurs for a Bernstein mode, then the upper frequency limit of the stop band is at a harmonic of the gyrofrequency. This result does not agree with the frequency limits of the attenuation bands observed during this flight, for which the gyrofrequency harmonic is generally *within* the attenuation band (see Figure 7).

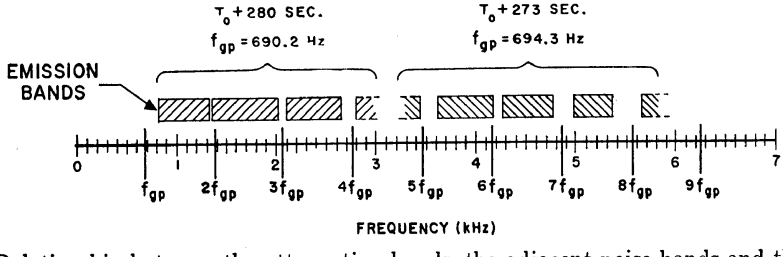

Fig. 7. Relationship between the attenuation bands, the adjacent noise bands and the proton gyrofrequency harmonics.

The failure of the Bernstein modes for a Maxwellian plasma to predict the correct cutoff frequencies may be accounted for in many ways. The velocity distribution function is almost certainly non-Maxwellian because the payload is flying through or near a proton aurora (L. A. Frank, personal communication), and the plasma is clearly unstable, therefore, non-Maxwellian. Also the wavelengths may be so small that Doppler shift effects are important.

2. *Wavelength.* Figures 4 and 6 illustrate that the attenuation bands are particularly clear on the short electric antennas. Comparison of the electric antenna noise intensities during the period from 271.0 to 274.0 seconds reveals that the high-band (650 Hz to 10 kHz) amplitudes for the short and long electric x-axis antennas are very nearly equal, about 1.0-mv ac potential difference between the antenna elements. These amplitudes strongly suggest that the wavelength of the noise observed is short compared with the long antenna length (3.16 meters), since the ac potential difference is independent of the antenna length. This wavelength is generally consistent with the characteristic length expected for gyrofrequency harmonic interactions, of the order of the mean gyroradius, or about 2 meters for thermal protons in the ionosphere.

Acknowledgments. We would like to thank Mr. R. D. Anderson and Mr. J. R. Cessna for their technical assistance in the design and construction of the payload and Mr. N. Peterson and Mr. V. Laurie at the Sounding Rockets Branch of Goddard Space Flight Center for their assistance and advice.

This research was supported by the National Aeronautics and Space Administration under contract NSR-16-001-025 and grant NGR-16-001-043, and by the Office of Naval Research under contract Nonr 1509(06).

References

Barrington, R. E., J. S. Belrose, and D. A. Keeley, Very low frequency noise bands observed by the Alouette 1 satellite, *J. Geophys. Res., 68,* 6539, 1963.

Bekefi, G., J. D. Coccoli, E. B. Hooper, and S. J. Buchsbaum, Microwave emission and absorption at cyclotron harmonics of a warm plasma, *Phys. Rev. Letters, 9,* 6, 1962.

Bernstein, I. B., Waves in a plasma in a magnetic field, *Phys. Rev., 109,* 10, 1958.

Brice, N. M., and R. L. Smith, A very low frequency plasma resonance, *Nature, 203,* 926, 1964.

Brice, N. M., and R. L. Smith, Lower hybrid resonance emissions, *J. Geophys. Res., 70,* 71, 1965.

Calvert, W., and G. B. Goe, Plasma resonances in the upper ionosphere, *J. Geophys. Res., 68,* 6113, 1963.

Crawford, F. W., Cyclotron harmonic waves in warm plasmas, *Radio Sci., 69D,* 789, 1965.

Crawford, F. W., and H. Weiss, Transmission characteristics of cyclotron harmonic waves in a plasma, *J. Nucl. Energy, Pt. C, 8,* 21, 1966.

Fejer, J. A., and W. Calvert, Resonance effects of electrostatic oscillations in the ionosphere, *J. Geophys. Res., 69,* 5049, 1964.

Frank, L. A., Initial observations of low-energy electrons in the earth's magnetosphere with OGO 3, *J. Geophys. Res., 72,* 185, 1967.

Fredricks, R. W., Structure of generalized low frequency Bernstein modes from the full electromagnetic dispersion relation, *TRW Systems Rept. 09485-6007-R000,* Redondo Beach, Calif., February 1968.

Gross, E. P., Plasma oscillations in a static magnetic field, *Phys. Rev., 82,* 232, 1951.

Gurnett, D. A., A satellite study of VLF hiss, *J. Geophys. Res., 71,* 5599, 1966.

Gurnett, D. A., A satellite observations of VLF emissions and their association with energetic charged particles, in *Earth's Particles and Fields, Proc. NATO Advanced Study Institute,* p. 127, Reinhold Book Co., New York, 1968.

Gurnett, D. A., and S. D. Shawhan, Determination of hydrogen ion concentration, electron density, and proton gyrofrequency from the dispersion of proton whistlers, *J. Geophys. Res., 71,* 741, 1966.

Iwai, A., J. Outsu, and Y. Tanaka, The observation of ELF-VLF radio noise with sounding rockets L-3-2, K-9M-6, *Proc. Res. Inst. Atmospherics Nagoya University, 13,* 1, January 1966.

Jensen, D. C., and J. C. Cain, An interim geomagnetic field (abstract), *J. Geophys. Res., 67,* 3568, 1968.

Laaspere, T., M. G. Morgan, and W. C. Johnson, Observations of lower hybrid resonance phenomena on the OGO 2 spacecraft, *J. Geophys. Res., 74,* 141, 1969.

Landauer, G., Generation of harmonics of the electron-gyrofrequency in a Penning discharge, *J. Nucl. Energy, Pt.C, 4,* 395, 1962.

McEwen, D. J., and R. E. Barrington, Some characteristics of the lower hybrid resonance noise bands observed by the Alouette 1 satellite, *Can. J. Phys., 45,* 13, 1967.

Morozumi, H. M., Diurnal variation of auroral zone geophysical disturbances, *Rept. Ionosphere and Space Res. Japan, 19,* 286, 1965.

Mosier, S. R., and D. A. Gurnett, Ionospheric observation of VLF electrostatic noise related to harmonics of the proton gyrofrequency, *Nature,* in press, 1969.

Sato, T., K. Matsuura, A. Miyahara, and S. Nagao, Experimental study of electrostatic ion

cyclotron waves in a plasma, *J. Phys. Soc. Japan, 23,* 378, 1967.

Shawhan, S. D., and D. A. Gurnett, VLF electric and magnetic fields observed with the Javelin 8.45 sounding rocket, *J. Geophys. Res., 73,* 5649, 1968.

Stix, T. H., *The Theory of Plasma Waves,* McGraw-Hill Book Company, New York, 1962.

Storey, L. R. O., Antenne electrique dipole pour preception TBF dans l'ionosphere, *L'onde Electrique,* t.SLV, No. 465, December 1965.

Sturrock, P. A., Dipole resonances in a homogeneous plasma in a magnetic field, *Phys. Fluids, 8,* 88, 1965.

Tanaka, S., and H. Kubo, Microwave radiation at cyclotron harmonics in a positive column, *Institute of Plasma Physics Rept. No. 23,* Nagoya University, Nagoya, Japan, 1964.

Watson, G. N., *A Treatis on the Theory of Bessel Functions,* Cambridge University Press, New York, 1922.

Yamamoto, T., and T. Suita, Excitation of ion cyclotron harmonic waves in a plasma by a perpendicular injected electron beam, *J. Phys. Soc. Japan, 24,* 933, 1968.

(Received March 4, 1969.)